Int J Adv Manuf Technol (2013) 68:209–216
DOI 10.1007/s00170-012-4721-z

ORIGINAL ARTICLE

Laser-arc hybrid welding of wrought to selective laser molten stainless steel

Giuseppe Casalino · Sabina Luisa Campanelli · Antonio Domenico Ludovico

Received: 22 October 2012 / Accepted: 29 December 2012 / Published online: 12 January 2013

Abstract Selective laser melting (SLM) is a successful tool-free powder additive technology. The success of this manufacturing process results from the possibility to create complex shape parts, with intrinsic engineered features and good mechanical properties. Joining SLM steel to similar or dissimilar steel can overcome some limitations of the product design like small dimension, undercut profile, and residual stress concentration. In this way, the range of applications of the SLM process can be broadened. In this paper, the hybrid laser welding of selective laser molten stainless steel was investigated. A high-power fiber laser was coupled to an electric arc and austenitic stainless steel wrought and SLM parts were welded together. The power and speed parameters were investigated. The joints were analyzed in terms of weld bead profile, microstructure, microhardness, and tensile test. The efficiency of the welding process was evaluated through the line energy input versus the weld molten area.

Keywords Fiber laser · Hybrid welding · Stainless steel · Selective laser molten powder

1 Introduction

As an alternative to powder metallurgy (P/M) technology, the selective laser molten process allows the creation of very complex geometries like deep helical cavities integrated with cooling channels and extractors, parts with unique design, and intrinsic engineered features that cannot be produced by conventional machining. [1]. However, the size of the selective laser melting (SLM) part is small and it is not possible to produce a large piece directly by the laser molten process. If the final object is very large and complicated, it may be necessary to build separate parts and joining or welding them together and with wrought pieces.

P/M iron based-based powder welding has been investigated using several techniques. Even if the welding is difficult due to the presence of porosities in their microstructure, the arc welding has given valuable results [2, 3]. For SLM powder, little knowledge of the effect of welding is available since almost no published literature exists on this subject. It is known that the SLM part is almost porosity free and in both cases of joining and welding it can require a finishing operation of the welding edges, which is due to the high roughness of the molten surface.

High-power laser beam welding is today an industrial joining process used as an alternative to the conventional arc welding processes. Both types of processes have their own advantages and disadvantages. The main advantages of the laser welding process are the low heat input and the high welding speed that produces a narrow and deep keyhole profile and a small heat-affected zone (HAZ). The arc welding process has high heat input and it is typically conduction limited, which produces wider and shallower welds at relatively low welding speed. However, the arc welding processes are

G. Casalino (✉) · S. L. Campanelli · A. D. Ludovico
DMMM, Politecnico di Bari, Viale Japigia 182,
70126 Bari, Italy
e-mail: g.casalino@poliba.it

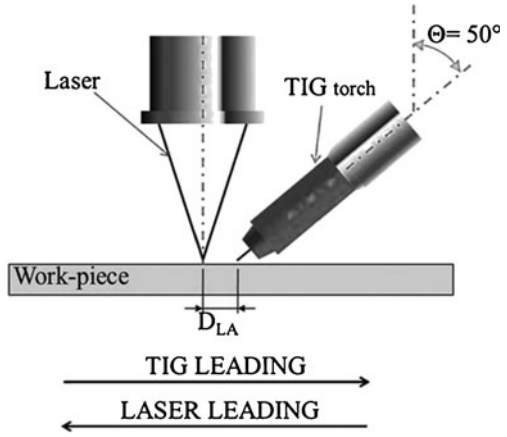

Fig. 1 Setup for laser arc hybrid welding

very efficient regarding the addition of filler material and therefore preferred when a joint gap is present due to unfinished condition of the welding edge.

Among the available laser source, the high power fiber laser has a compact design and good beam quality. It can deliver several kilowatts of power and has an extended working life. Their wavelength is near to the Nd:YAG, which implicates a good absorptivity by a wide range of materials. High power fiber laser can be used for deep penetration welding for a variety of materials. Quintino et al. [4] demonstrated that the operating costs are lower than those of CO_2 and Nd:YAG. However, a great shortfall of the fiber laser welding process is the precise fit-up requirement for the joint geometry that depends on the small beam focus diameter.

The laser and the conventional arc can be combined in such a way that they interact to form a new welding process that is the laser arc hybrid welding process (LAHW). The basics of this process were illustrated by many papers that show that the LAHW process offers significant advantages including higher welding speeds, reduced total heat input, increased arc stability, gap bridging ability, and deep fused zone. Classification, characteristics, and applications of hybrid laser beam welding were given by Mahrle and Beyer [5].

The primary scope of this paper was to discuss and explain the capacity of the hybrid laser welding to produce an effective and efficient butt weld between selective laser molten and wrought stainless steels. A fiber laser was coupled with a tungsten inert gas (TIG) electric arc in order both to overcome the precise fit-up requirement for the joint geometry, which depends on the small beam focus diameter, and to exploit the beam deep penetration.

Several experiments were made on dissimilar AISI 316 L butt welds. Two configurations of the welding source were studied; they were the laser-leading (La-TIG) and the TIG-leading (TIG-La). In the former, the laser preceded and in the latter followed the arc with respect to the welding direction (Fig. 1).

The effects of the laser power, travel speed, arc current, and arc voltage were tested. The base plates were welded without any surface preparation. The joints were characterized in terms of the transverse cross-section defectiveness, the microstructure, the microhardness, and

Table 1 Chemical composition of materials

Elements	AISI 316 L powders % wt.	AISI 316 L Wrought % wt.
Cr	17	16.63
Ni	12	10
C	0.030 max	0.022
Si	0.5	0.41
Mn	1.5	1.31
Mo	2.5	2.0
Fe	Balance	Balance

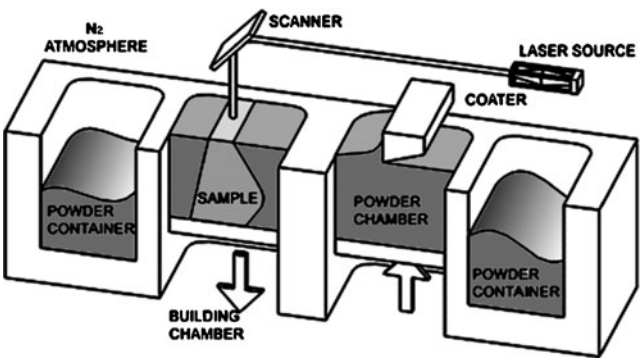

Fig. 2 SLM equipment

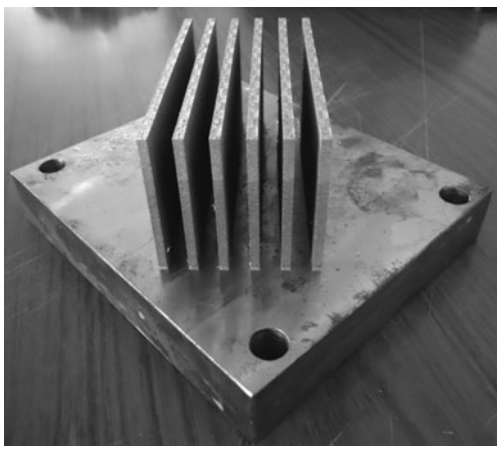

Fig. 3 SLM plates

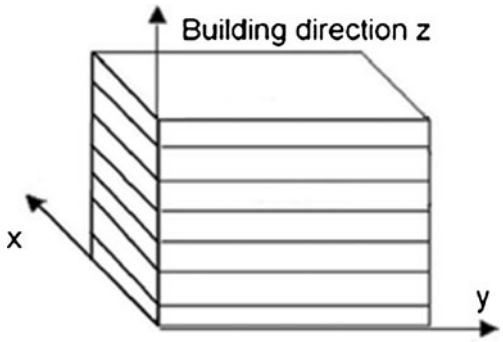

Fig. 4 Roughness measurement directions

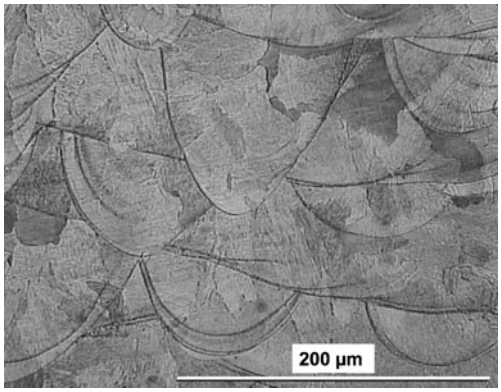

Fig. 5 SLM transverse cross-section

the tensile test. The efficiency of the welding process was evaluated by the ratio between the area of the fused zone and line energy.

2 Description of the hybrid laser welding process

LAHW is a versatile welding technique. In fact, it tends to maximize benefits and minimize the drawbacks that characterize each combined welding process. The applications vary from thick section of low alloy high strength steels [6] to light alloys like aluminum [7] and titanium [8]. Some authors investigated heterogeneous welding between steel and aluminum [9] and between copper and steel [10]. Unfortunately, when the two techniques are combined the number of process parameters is rather large and therefore the welding process is rather difficult to optimize [11].

The type of laser source used affects the distance between the torch and the laser, which is generally few millimeters. Petring et al. [12] found that the Nd:YAG laser radiation, due to a low interaction with the arc plasma, allows a closer distance from the arc than CO_2 laser radiation. The distance between the sources influences the mixing phenomena between the deep and narrow molten pool deriving from the laser and the wide and superficial molten pool deriving from the arc. The optimal distance in hybrid welding of carbon steel depends on many other factors, such as laser power, torch angle, and arc parameters like size, current, voltage, and pulsing [13]. The laser reflectivity of the metal plates is reduced when the metal is heated by the arc as it was shown for the titanium [14].

Table 2 Average roughness values along *x*-, *y*-, and *z*-axis

	X direction	*Y* direction	*Z* direction
Ra (µm)	20.8	23.4	17.2

Some authors investigated the shielding gas parameters, i.e., the composition and the protecting method, and the laser beam focal position effect on the weld microstructure and mechanical strength [15, 16].

When constant laser power and welding speed is used, the higher the arc current the deeper must be the focal point below the surface of the workpiece to achieve good penetration [17]. In fact, if the arc current rises, the depth of the weld pool grows up. If the plane of the laser focus is placed on the workpiece surface, it does not act inside the resulting weld pool and so the maximum penetration cannot be reached. In conclusion, the maximum weld penetration for the hybrid laser arc process is generally obtained when the laser beam is focused below the top sheet surface, with a value related to welding current.

Arias et al. [18] studied the laser Nd:YAG TIG hybrid welding of very thin 316 L stainless steel sheets (0.4–0.8 mm thick) in a butt joint configuration. They found that the laser melted pool stabilizes the TIG arc and a laser trailing arrangement allows welding speeds until 15 m/min. Moreover, the full penetration joints can be successfully produced minimizing the TIG current

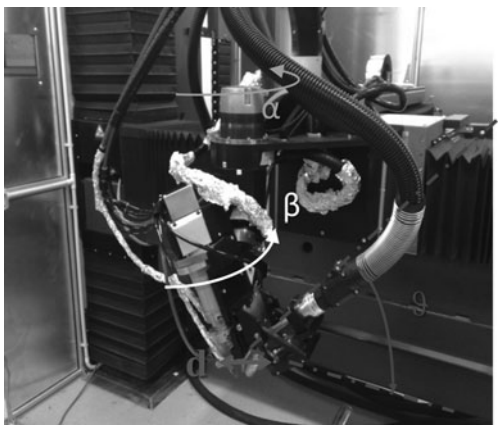

Fig. 6 Hybrid laser-TIG equipment used for experiments

Table 3 Plan of the experiments

La-TIG	TIG-La	Current (A)	Voltage (V)	Travel speed (m/min)	Laser power (W)
1	4	150	24.7	3	2,000
2	5	150	24.7	3	2,500
3	6	200	26.2	6.5	4,000

and using argon as a shielding gas. A significant improvement of the melting efficiency was achieved with the combined action of plasma arc and laser beam [19].

3 Description of the selective laser melting process

The SLM technology creates fully functional parts directly from metal powders without using any intermediate binders or any additional processing step after the laser sintering operation [20]. The equipment consists (Fig. 2) of a control system, a coater or roller, a laser source, a scanning system, a working chamber, a powder chamber which is the reservoir for the powder, a controlled atmosphere chamber, and some rooms filled with excess powder.

The working chamber is filled with a gas (Ar or N_2 depending on the processed materials), to minimize both the oxidation and degradation of the molten metal. The coater deposits, in uniform way, the powder on the building chamber. The laser beam selectively scans and melts the surface of the powder. When the first two-dimensional layer is created the process is repeated until the object is built layer by layer.

Following different manufacturing strategies, the AISI 316 stainless steel was processed by selective laser melting [21]. The metallurgical feature of SLM of stainless steel and its surface morphology were investigated by Jinhui et al.

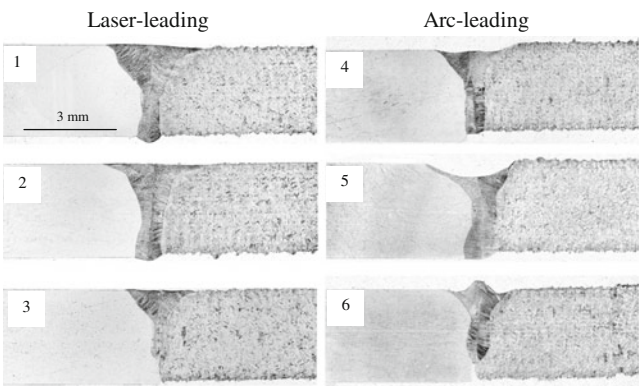

Fig. 7 Weld bead profiles for La-TIG and TIG-La configurations (see Table 3 for reference)

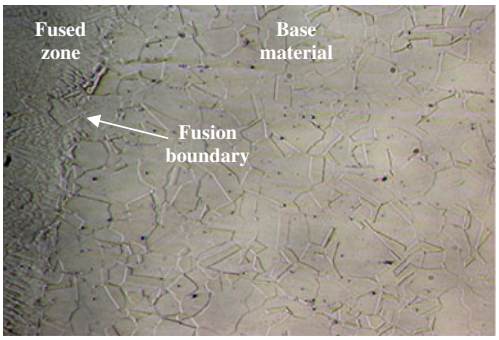

Fig. 8 Fusion boundary on the wrought steel side (50×)

[22]. An extremely fine microstructure is produced by the very rapid cooling and multiple grain directions happen due to the variable heat transfer direction. The mechanical strength of laser molten steel is better than that of the annealed steel.

4 Experimental procedures

4.1 Design and fabrication of SLM parts

Since the work of Casavola et al. [23] showed that the melting/solidification mechanism generates highly variable thermal residual stresses, SLM parts were produced using an island scansion strategy. The Nd:YAG laser was used for the part build-up. The power was set to 100 W, the layer thickness to 30 μm and the scanning speed to 200 mm/s. The focus diameter was 0.2 mm.

The chemical composition of AISI 316 L powders and wrought steels are given in Table 1. The relative density, measured with the Archimedes method, was higher than 99 %. Figure 3 shows the SLM samples, which were built on a support plate along the vertical direction. The built plates were not post-treated.

Roughness was measured on all samples along the *x*, *y*, and *z* directions as shown in Fig. 4. Table 2 contains the average values along the three axes.

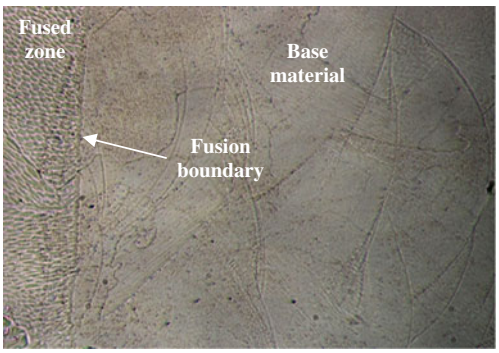

Fig. 9 Fusion boundary on the SLM steel side (50×)

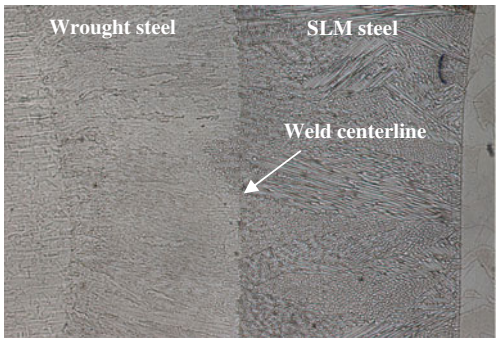

Fig. 10 Transverse cross-section of the weld keyhole (10×)

Figure 5 shows a micrograph of the cross-section of an SLM parts with the typical layer by layer structure. The cut was parallel to the SLM building direction. The picture also highlights the approximately parabolic shape of the molten/resolidified zone.

4.2 Experimental set up and plan of the experiments

In this study, a five-axis welding machine was used (Fig. 6). It was characterized by three-axis controlled robotic units (*x*-*y*-*z*), focus head with dual-axis control (α–β) and a fixed work plan. The maximum linear speed along *x*-*y*-*z* axis was 20 m/min and the maximum rotational speed along the axis α and β 66 rpm.

The welding machine was equipped with an ytterbium laser source with a maximum power of 4 kW and a wavelength of 1,070 nm. The TIG source was characterized by a maximum current of 500 A in continuous mode.

The combined welding source consisted of a laser source and a TIG torch, which was tilted by a θ angle respect to the workpiece surface (Fig. 1). The distance between the tungsten electrode tip and the laser beam axis was indicated with laser arc distance (D_{LA}). The position of the two sources respect to the welding direction determined two different welding setups: laser leading (La-TIG) in which the laser is located before the TIG and TIG leading (TIG-La) where the TIG is the first acting source.

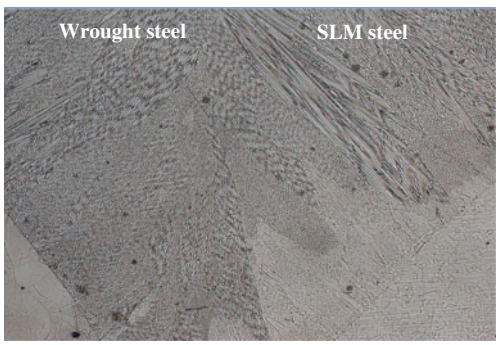

Fig. 11 Transverse cross section of the weld crown (10×)

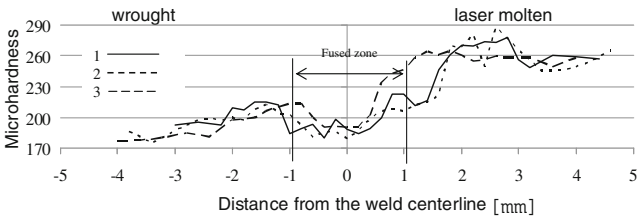

Fig. 12 Microhardness upper profile for laser leading samples (*1*, *2*, *3*)

Table 3 shows the process parameters at-a-glance for both configurations La-TIG (samples 1, 2, and 3) and TIG-La (samples 4, 5, and 6). The tests were conducted on 3 mm dissimilar thick butt weld. Argon was used as shielding gas on the TIG torch while no shielding gas was used for the laser beam; a thin flow of compressed air protected the optics.

For all configurations, the D_{LA} was kept constant and equal to 3 mm; α and β angles were set to 0 and the inclination angle of the TIG torch was set to 50°.

5 Results and discussion

5.1 Weld bead shape and microstructure

The welds were cut at the cross-section and then cut, polished, and etched. Glyceregia etching reagent (5 ml HNO_3, 10 ml glycerol, 15 ml HCl) was used to reveal the metallurgical structure. Figure 7 displays the weld transverse cross-sections obtained using the process parameters showed in Table 3.

The transverse cross-sections demonstrated that the fused zone had a “nail” shape. The crown was determined mainly by the surface tension, which depends on the arc source. The penetration depth during keyhole mode laser welding was influenced primarily by the presence of the keyhole, which was due to the laser beam penetration. The reinforcement was observed for sample 6, which presented a small hill profile at the weld centerline with slight undercut on both sides.

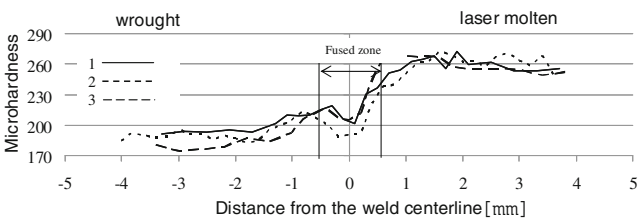

Fig. 13 Microhardness lower profile for laser leading samples (*1*, *2*, *3*)

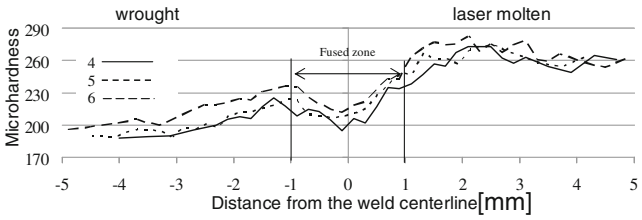

Fig. 14 Microhardness upper profile for TIG leading samples (*1*, *2*, *3*)

For samples 3 and 6, which were produced using the highest welding speed, the penetration was incomplete. Underfill was observed for samples 4 and 5. This can be explained with the fact that during La-TIG welding, a greater amount of laser energy was used to melt the base metal, which led to lower evaporative losses and expulsion of metal. In contrast, during TIG-La, the laser beam may cause significant expulsion of liquid metal and a heavy loss of evaporative elements from the melted base metal.

At the same time, under the actions of surface tension and hydrostatic pressure, the molten metal on the keyhole wall has a tendency to flow downward along the keyhole wall. The wrought steel contained equiaxed grains of austenite with occasional twinning and ferrite at the grain boundary. SLM parts had the typical layer by layer structure with the characteristic parabolic shape of the molten zone.

On the side of the wrought steel the typical cellular growth at the fusion boundary was observed. HAZ was not resolved (Fig. 8) since it was very thin as it was also found by Yan et al. [24] in their study on microstructure of stainless steel TIG-CO_2 laser hybrid welding.

The cellular solidification with ferrite precipitation at the grain borderline was established near the fusion boundary on the SLM steel (Fig. 9). It is common that the primary grain size of the weld metal is determined by the grain size of the solid metal at the fusion boundary [25]. The grain size on SLM side was finer than that of wrought steel grain.

The rapid solidification of stainless steel was followed by columnar growth (Fig. 10), as it was demonstrated for the capacitative discharge welding [26]. SLM

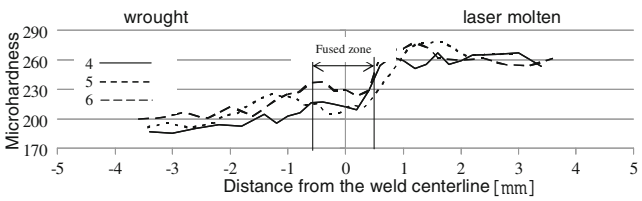

Fig. 15 Microhardness lower profile for TIG leading samples (*4*, *5*, *6*)

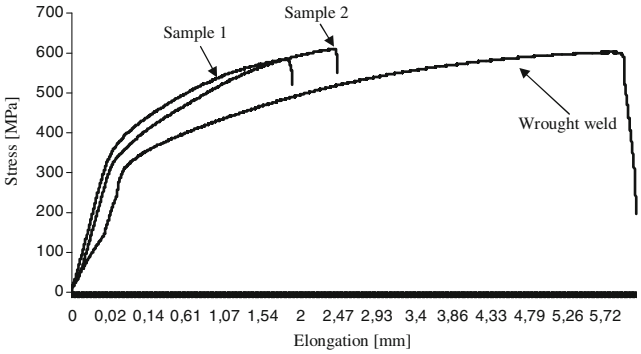

Fig. 16 Tensile test diagrams

side of fused zone presented also a random grain orientation due to the small grain and the element precipitation at the border of the grain during the SLM process. The grain of the wrought steel-fused zone was bigger and presented a regular centerline orientation.

The increase in the ratio between the temperature gradient and the rate of advance produced a columnar dendrite growth toward weld centerline with random grain orientation (weld crown in Fig. 11). The weld centerline was disrupted by the multi-oriented growth of the grains from the SLM to the wrought side of the fused zone. The primary dendrites showed a darker phase.

5.2 Microhardness and tensile test

Figures 12, 13, 14, and 15 show the Vickers hardness distribution at the top (0.5 mm from the surface) and at the bottom (0.5 mm from the back) of the weld for both arc and laser leading configurations. The measurements were taken for all the joints using a 200 g indentation load.

The microhardness of the annealed and the SLM steels were 190 and 260 HV, respectively. At the weld top, the microhardness in the fused zone was as low as that of the annealed steel in the laser leading configuration and slightly higher in the arc leading one. The SLM side was little affected by the thermal cycle. The width of the fused zone was about 2 mm in both configurations of the welding source.

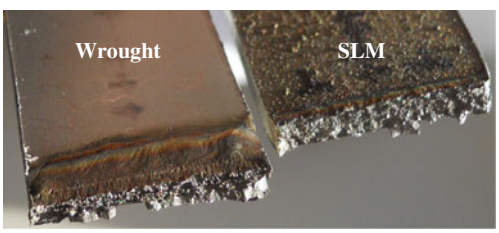

Fig. 17 Fracture surface of the sample 1

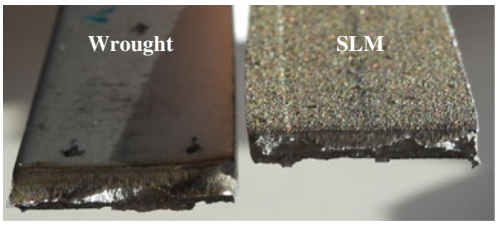

Fig. 18 Fracture surface of the sample 2

At the weld bottom, the microhardness had the same distribution as at the weld top but with slightly higher values and a fused zone as wide as 1 mm. Again, the SLM side was little affected by the thermal cycle.

The microhardness distribution was determined mostly by the arc effect at the weld top and by laser keyhole at the bottom. A little difference was observed between the arc and laser leading configurations.

The tensile test was performed only for the defect free and full penetration samples 1 and 2, which were obtained in the laser leading configuration. Rectangular samples of the weld taken along the perpendicular direction to the welding line were tensile tested. The samples were 3 mm thick, 10 mm wide, and 100 mm long. The loading direction was parallel to the SLS build-up direction. Figure 16 illustrates the tensile test results for the two dissimilar welds samples 1 and 2 (see Table 3 for process parameters) and a hybrid laser weld made of annealed wrought stainless steel.

The mechanical strength was as high as that of the wrought material. Otherwise, the elongation was lower for the dissimilar welds than for the similar one.

The fracture appeared in the SLS side. For the sample 1 it was a brittle rupture (Fig. 17). The sample 2 showed sign of a brittle to ductile rupture (Fig. 18). Figure 19 shows the fracture surfaces of the annealed wrought steel.

The behavior of the dissimilar weld was good in terms of mechanical strength. The tensile properties were affected by the microhardness distribution and in particular by the sharp elevation in the interface between the fused zone and SLM. The elongation of the dissimilar weld could be improved by an annealing heat treatment of the SLM steel.

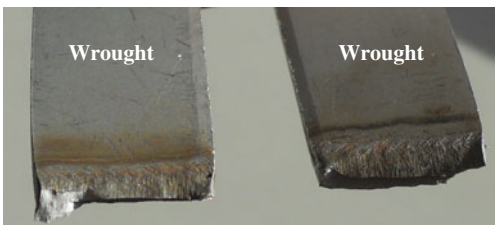

Fig. 19 Fracture surface of the wrought sample

Table 4 Data related to the welding efficiency analysis

Welds	LE_{LA}	LE_A	LE_{TOT}	LAER
Samples 1 and 4	40	74.1	114.1	0.54
Samples 2 and 5	50	74.1	124.1	0.67
Samples 3 and 6	36.9	48.4	85.3	0.76

5.3 Energy welding efficiency

The energy welding efficiency is the ratio between the molten area in the transverse cross section and line energy input. The line energy (in Joules per millimeter) was calculated for both the arc and the laser sources and was given by Eq. 1 for the laser (LE_{LA}) and by Eq. 2 for the arc (LE_A)

$$LE_{LA} = \frac{P}{v} \tag{1}$$

$$LE_A = \frac{V \cdot I}{v} \tag{2}$$

where P is the laser power, v is the welding speed, V is the arc voltage, and I is the arc current.

The total energy line (LE_{TOT}) was given by the sum of the line energies. Moreover, the laser to arc energy ratio (LAER) was calculated as LE_{LA}/LE_A. Table 4 shows the values of LE_{LA}, LE_A, LE_{TOT}, and LAER for both the laser and the arc leading configurations.

The energy efficiency of the laser leading configuration was sensitive and had negative correlation to the LAER. The energy efficiency of the arc leading configuration showed a slight positive correlation to the LAER (Fig. 20). The most efficient weld was obtained with the laser leading configuration with a 0.54 LAER.

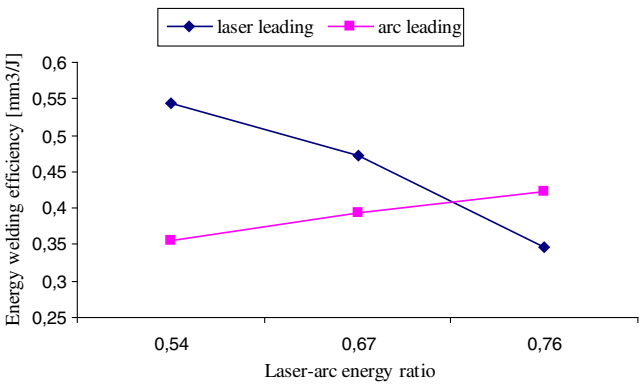

Fig. 20 Plot of the energy welding efficiency versus the laser arc energy ratio

6 Conclusion

In this paper, the effects of the hybrid laser welding on wrought to SLM stainless steel weld were studied. Electric and laser parameters were tested in both the laser leading and arc leading configurations.

The obtained weld microstructure was composed by cellular and columnar growth with a random orientation of the grains in the SLM side of the fused zone and in the weld crown. The explanation was the small grain and the element precipitation at the border of the grain during the SLM process. The laser leading configuration produced defective-free welds.

The microhardness distribution was determined mostly by the arc effect at the weld top and by the laser keyhole at the bottom. A little difference was observed between the arc and the laser leading configurations. The tensile test showed good strength but low elongation. Annealing of the weld can improve the elongation of the weld. The energy efficiency was higher in the laser leading configuration and for the lower laser to arc energy ratio. Altogether, a sound and energy efficient weld can be fabricated using the laser leading configuration and low laser to arc energy ratio.

Eventually, this investigation showed the feasibility of the welding of the selective laser molten stainless steel by fiber laser-arc hybrid in terms of effectiveness and efficiency. Hence, the laser additive process of stainless steel can gain more flexibility in case of the product design requires the build-up of separate parts and then welding them both together and with wrought components.

The future direction of this research will be the study of the interaction between the SLM and the welding parameters. The heat treatment of the weld will be also investigated. Then, the optimization of hybrid welding of SLM stainless steel will be possible.

References

1. Campanelli SL, Contuzzi N, Angelastro A, Ludovico AD (2010). In: Meng Joo Er (ed) New trends in technologies: devices, computer, communication and industrial systems, Sciyo, Rijeka, pp. 233–252
2. Liu S, Zhang H, Jiandong H, Shi Y (2013) Microstructure of laser-MAG hybrid welds of sintered P/M steel. J Mater Eng Perform 22:251–257
3. Correa EO, Costa SC, Santos JN (2008) Weldability of iron-based powder metal materials using pulsed plasma arc welding process. J Mat Pro Tech 198:323–329
4. Quintino L, Costa A, Miranda R, Yapp D, Kumar V, Kong CJ (2007) Welding with high power fiber lasers—a preliminary study. Mater Des 28:1231–1237
5. Mahrle A, Beyer E (2006) Hybrid laser beam welding—classification, characteristics, and applications. J Laser Appl 18(3):169–180
6. Cao X, Wanjara P, Huang J, Munro C, Nolting A (2011) Hybrid fiber laser—arc welding of thick section high strength low alloy steel. Mater Des 32:3399–3413
7. Casalino G, Lobifaro F (2005) Process parameters effects on Al–Mg alloys MIG-laser CO_2 welding. Proceedings of ICALEO 2005. Miami, USA, pp. 1062–1068
8. Cui L, Kutusna M, Simizu T, Horio K (2009) Fiber laser-GMA hybrid welding of commercially pure titanium. Mater Des 30 (1):109–114
9. Casalino G, Rella C (2005) MIG-laser combined welding of aluminum alloy to 304 stainless steel. Proceedings of ICALEO 2005. Orlando, USA, pp. 287–292
10. Asai S, Ogawa T, Ishizaki Y, Minemura T, Minami H, Miyazaki S (2012) Application of plasma MIG hybrid welding to dissimilar joints between copper and steel. Weld World 56(1–2):37–42
11. Le Guen E, Fabbro R, Carin M, Coste F, Le Masson P (2011) Analysis of hybrid Nd:Yag laser-MAG arc welding processes. Opt Laser Technol 43:1155
12. Petring D, Fuhrmann C, Wolf N, Poprawe R (2007) Progress in laser-MAG hybrid welding of high-strength steels up to 30 mm thickness. Proceedings of ICALEO 2007. Orlando, USA, pp. 300–307
13. Kutsuna M, Chen L (2002) Interaction of both plasmas in CO_2 laser-MAG hybrid welding of carbon steel. Proceedings of the First International Symposium on High-Power Laser Macroprocessing. Osaka, Japan, pp. 341–346
14. Li C, Muneharua K, Takao S, Kouji H (2009) Fiber laser-GMA hybrid welding of commercially pure titanium. Mater Des 30:109
15. Gao M, Zeng X, Hu Q (2007) Effects of gas shielding parameters on weld penetration of CO_2 laser-TIG hybrid welding, J Mater Process Tech 184:177–182
16. Sathiya P, Mishra K, Shanmugarajan B (2012) Effect of shielding gases on microstructure and mechanical properties of super austenitic stainless steel by hybrid welding. Mater Des 33:203–212
17. El Rayes M, Walz C, Sepold G (2004) The influence of various hybrid welding parameters on bead geometry. Weld J 83(5):147–153s
18. Arias JL, Romero P, Vandewynckèle A, Vázquez J (2005) Laser-TIG hybrid welding of very thin austenitic stainless steel sheets. Proceedings of ICALEO 2005. Miami, USA, pp. 104–107
19. Mahrle A, Schnick M, Rose S, Demuth C, Beyer E, Füssel U (2011) Process characteristics of fibre-laser-assisted plasma arc welding. J Phys D App Phys 44
20. Kruth JP, Froyen L, Van Vaerenbergh J, Mercelis P, Romboutsb M, Lauwers B (2004) Selective laser melting of iron-based powder. J Mater Process Technol 149:616–622
21. Tolosa I, Garciandía F, Zubiri F, Zapirain F, Esnaola A (2010) A study of mechanical properties of AISI 316 stainless steel processed by "selective laser melting, following different manufacturing strategies". Int Jour Adv Manuf Technol 51:639–648
22. Jinhui L, Ruidi L, Wenxian Z, Liding F, Huashan Y (2010) Study on formation of surface and microstructure of stainless steel part produced by selective laser melting. Mater Sci Technol 26(10):1259–1264
23. Casavola C, Campanelli SL, Pappalettere C (2009) Preliminary investigation on distribution of residual stress generated by the selective laser melting process. J Strain Anal Eng Des 44:93–104
24. Yan J, Gao M, Zeng X (2010) Study on microstructure and mechanical properties of 304 stainless steel joints by TIG, laser and laser-TIG hybrid welding. Opt Laser Eng 48:512–517
25. Lancaster JF (1993) Metallurgy of welding, 5th edn. Chapman & Hall, London, p 148
26. Casalino G, Panella FW (2007) Microstructural analysis of AISI 304 bars welded with high speed pulsed discharges. J Mater Process Technol 191:149–152